Self-calibration of Scheimpflug cameras: an easy protocol

Meas. Sci. Technol. **18** (2007) 2616–2622 doi:10.1088/0957-0233/18/8/037

Self-calibration of Scheimpflug cameras: an easy protocol

H Louhichi[1,2], T Fournel[1], J M Lavest[3] and H Ben Aissia[2]

[1] Laboratoire Traitement du Signal et Instrumentation, UMR 5516 CNRS, Université Jean Monnet, 18 rue du Pr B Lauras, 42000 Saint Etienne, France
[2] Unité de Métrologie en Mécanique des Fluides et Thermiques, UR 11-17, Université de Monastir, Iben Eljazzar, 5019 Monastir, Tunisia
[3] Laboratoire de Sciences des Materiaux pour l'Electronique et d'Automatique, UMR 6602 CNRS, Université Blaise Pascal, 24 avenue des Landais, 63177 Aubiere Cedex, France

E-mail: fournel@univ-st-etienne.fr

Received 4 August 2006, in final form 11 April 2007
Published 11 July 2007
Online at stacks.iop.org/MST/18/2616

Abstract
The problem of the self-calibration of Scheimpflug cameras is addressed. The approach aims to calibrate by handpositioning a roughly-known calibration pattern, thanks to a bundle adjustment technique. The purpose of this paper is to design an easy protocol accordingly. A simple motion of the calibration target is introduced and a minimal number of recordings are obtained from the simulated data. The precision required for the calibration pattern is also discussed. Finally, the suggested protocol is tested in real conditions, especially in the stereo particle image velocimetry configuration.

Keywords: self-calibration, calibration, Scheimpflug condition, stereoscopic particle image velocimetry

1. Introduction

The Scheimpflug condition is used for focusing a video camera during oblique viewing at low-aperture numbers. This condition is performed by tilting the sensor (or the lens) such that the object plane, the lens plane and the image plane intersect in a common line (figure 1). This configuration is used in stereoscopic particle image velocimetry (SPIV) for measuring the three components of the velocity field in a section of a flow [1, 2]. It allows a high view angle with respect to the laser sheet illuminating the studied section and so a large triangulation angle between the optical axes of the cameras [3]. The three velocity components are reconstructed from back-projections onto a reference plane defined at the calibration stage.

The first task of calibration is to recover the parameters required for reconstruction from views of the calibration target: the coefficients of the projection functions which are usually considered as polynomial [4], rational polynomial [5] or bicubic splines [6]. Some additional parameters, mainly triangulation angles, are also to be recovered when the previous functions are 2D–2D functions, mapping the object plane onto the image recording planes [5]. A target known with precision is used for this purpose. Multi-level targets on which different z-positions are present are available for the special case of StereoPIV calibration [7]. When using a planar target, it is classically accurately moved to different z-positions as in [8]. A single z-position can be sufficient provided that some parameters such as the focal length and sensor pixel pitches of each PIV camera are known [9]. Usually, the calibration target is accurately positioned with respect to the laser plane (the measurement plane) and the misalignment between the reference plane and the laser plane [5, 10–12] is corrected from the disparity vector map computed by cross-correlating particle images of cameras 1 and 2, recorded at time t.

Self-calibration was suggested in [13] in order to allow handpositioning of the calibration target. Calibration becomes easier as accurate positioning is no longer required. An efficient procedure for self-calibration is developed in [14]. It is based on fitting a camera pinhole model to the two cameras until the disparity vector map converges towards a null map. This iterative correction of the camera models (after triangulation and plane fit) results from their first fit using a single or multiple views of a well-known 3D calibration plate. However, in the case where several sizes of the view field have to be considered, one would like to calibrate with low-cost

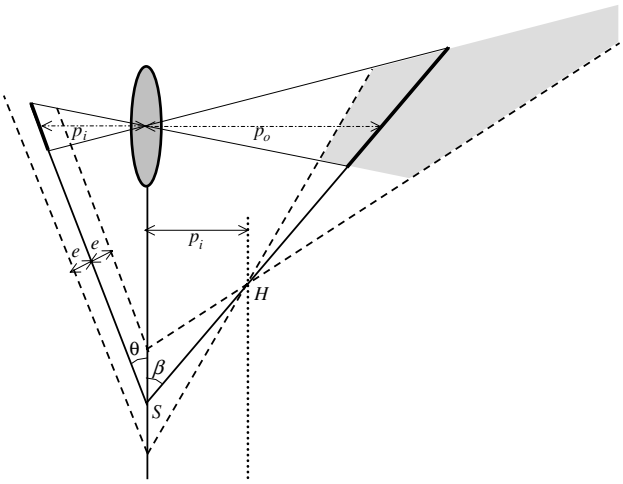

Figure 1. Cross-section of the Scheimpflug set-up: the object plane (viewed under an angle β), the lens plane and the image plane (rotated by an angle θ) intersect in the Scheimpflug line (S). The near and far limits of the depth of field (dashed lines) intersect in the Hinge line (H). These planes are respectively conjugated to limiting planes parallel and at either side of the image plane at a distance e given by the length of acceptable confusion: for images focused at either of the limiting planes, the shape of confusion on the image plane will be the maximum allowable.

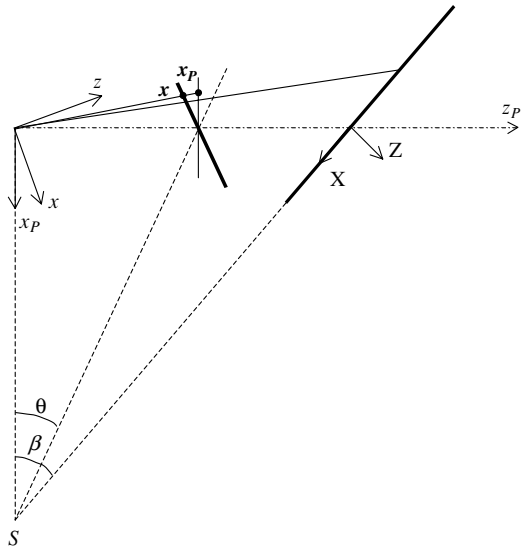

Figure 2. Coordinate systems in the Scheimpflug condition according to the 'painter convention': the image plane is placed in front of the projection centre C by symmetry with respect to this point.

targets well-adapted to the different sizes. In such cases one would like to use roughly-known targets, for example, some pieces of printed paper, without accurate knowledge of the calibration pattern. This scheme can be carried out by fitting the calibration points together with the camera parameters by least mean squares [13]. It works because of the redundancy obtained from multiple viewing of the target (as the intrinsic camera parameters remain constant) and because of subpixel detection of the images of the calibration points [15].

This paper aims to design an easy protocol for this self-calibration when viewing in air in the Scheimpflug condition. It concerns the two following points: definition of the degree of precision required in the knowledge of the calibration pattern and determination of some relevant sets of views. The technique used for fitting both the camera parameters and the calibration points is a technique of bundle adjustment [15] described in section 2. It is based on fitting the bundles of the rays connecting the calibration points with their images accurately detected in the views. The associated protocol is presented in section 3 and refined from certain simulations in section 4.1. Finally, the protocol is tested in real conditions in section 4.2.

2. Bundle adjustment technique in the Scheimpflug condition

Bundle adjustment is a videogrammetric technique used for (self-)calibrating cameras or recovering the 3D structure of a scene [16]. Each projection function corresponds here to a camera model determined by the intrinsic and extrinsic camera parameters. The intrinsic ones are the parameters of the camera itself. The extrinsic ones are the parameters of the location of the camera with respect to the world coordinate system. The distinction between the intrinsic and extrinsic parameters allows high redundancy when recording a set of views of the target. The difference between the number of equations and the number of unknown parameters increases with the number of views because the intrinsic parameters remain constant. Redundancy becomes high enough to self-calibrate, i.e. to introduce the coordinates of the calibration points into the vector $\mathbf{\Phi}$ of the parameters to be adjusted by least mean squares. The calibration points are estimated simultaneously with the camera parameters by minimizing the image residual errors

$$\begin{cases} \varepsilon_{\mathrm{u}} = u - \mathrm{u} \\ \varepsilon_{\mathrm{v}} = v - \mathrm{v}, \end{cases} \tag{1}$$

where (u, v) are the pixel coordinates of the projection of a calibration point (given by the camera model) and (u, v) are the measured ones.

2.1. Camera model

The camera model has to be determined as coordinates (u, v) in (1) which depends on its parameters. The Scheimpflug camera model can be derived from the pinhole one. According to the pinhole model, point $\mathbf{X} = (X, Y, Z, 1)^{\mathrm{T}}$ (in the world coordinate system) is projected to $\mathbf{x_P} = (x, y, z, 1)^{\mathrm{T}}$ in the (first) camera coordinate system (figure 2) as

$$\mathbf{x_P} \sim \mathbf{P_P} \begin{pmatrix} \mathbf{R_P} & \mathbf{t_P} \\ \mathbf{0}^{\mathrm{T}} & 1 \end{pmatrix} \mathbf{X} + \delta\mathbf{x}, \tag{2}$$

where the equivalence relation denoted by symbol $\sim$ means equality up to a non-zero scale factor. $\mathbf{R_P}$ and $\mathbf{t_P}$ are the rotation and translation matrices, respectively, connecting the world coordinate system to the camera coordinate system, $\mathbf{P_P}$ is the perspective projection to the frontal plane and $\delta\mathbf{x}$ is the distortion term. In standard conditions, distortions are usually reduced to radial ones given by adimensional coefficients a_1, a_2, a_3 [17] as follows:

$$\begin{cases} \delta x = x(a_1 r^2 + a_2 r^4 + a_3 r^6) \\ \delta y = y(a_1 r^2 + a_2 r^4 + a_3 r^6), \end{cases} \tag{3}$$

where $r = \sqrt{x^2 + y^2}/p_i$ is the normalized distance from the image centre.

The Scheimpflug model includes the tilt angle θ of the image plane (figure 1) as the supplementary parameter. The tilt is performed according to the Scheimpflug condition. This condition is satisfied when the image plane, the lens plane and the object plane intersect in a common line. It ensures that the conjugation formula $\frac{1}{f} = \frac{1}{p_i} + \frac{1}{p_o}$ is verified. With the nominal magnification $M = \frac{p_i}{p_o}$ and view angle β, the tilt θ is given by (figure 1)

$$\theta = \arctan(M \tan(\beta)). \tag{4}$$

Image $\mathbf{x}$ can be deduced from $\mathbf{x_P}$ by

$$\mathbf{x} \sim \begin{pmatrix} \mathbf{R_S} & \mathbf{0} \\ \mathbf{0}^{\mathrm{T}} & 1 \end{pmatrix} \mathbf{P_S}\, \mathbf{x_P}, \tag{5}$$

where $\mathbf{P_S}$ is the perspective projection in the image plane and $\mathbf{R_S}$ is the (Scheimpflug) rotation of the camera coordinate system which leads the optical axis to merge in the normal of the tilted image plane.

The tilted optical axis intersects the image plane in the Scheimpflug image centre $\mathbf{x}_0$ and defines an ideal pinhole camera without distortions:

$$\mathbf{x} \sim \mathbf{P_{PS}} \begin{pmatrix} \mathbf{R_{PS}} & \mathbf{t} \\ \mathbf{0}^{\mathrm{T}} & 1 \end{pmatrix} \mathbf{X}, \tag{6}$$

where $\mathbf{P_{PS}} = \mathbf{P_S P_P}$ and $\mathbf{R_{PS}} = \mathbf{R_S R_P}$.

The Scheimpflug camera model cannot be reduced to the ideal pinhole model unless the view angle is low or distortions are neglected. Indeed, when the view angle is inferior to 10°–15°, the tilt θ is 1° at maximum, and in practice it cannot be optimized separately from the view angle. Otherwise, by neglecting distortions in (6), the Scheimpflug rotation can commute with projection matrices.

2.2. Multi-views and optimization of calibration points

To summarize, there are eight intrinsic parameters: the tilt angle θ and the pinhole parameters which are the image distances expressed in pixels: $p_{i\,x} = \frac{p_i}{d_x}$ and $p_{i\,y} = \frac{p_i}{d_y}$, where d_x, d_y are the x- and y-size of the pixels, pixel coordinates (u_0, v_0) of the image centre and distortion coefficients a_1, a_2, a_3. Multi-viewing leads to m different positions of the target giving $6m$ extrinsic parameters: Euler angles $\alpha^{(j)}$, $\beta^{(j)}$, $\gamma^{(j)}$ of rotation $\mathbf{R_P}$ and components $t_x^{(j)}$, $t_y^{(j)}$, $t_z^{(j)}$ of translation $\mathbf{t_P}$. By introducing coordinates (X_i, Y_i, Z_i) of the n calibration points, vector $\mathbf{\Phi}$ of the parameters to be optimized is given by

$$\begin{aligned} \mathbf{\Phi}_{8+6m+3n} = \big(&p_{i\,x}, p_{i\,y}, u_0, v_0, a_1, a_2, a_3, \theta, \\ &\alpha^{(1)}, \beta^{(1)}, \gamma^{(1)}, t_x^{(1)}, t_y^{(1)}, t_z^{(1)}, \ldots, \\ &\alpha^{(m)}, \beta^{(m)}, \gamma^{(m)}, t_x^{(m)}, t_y^{(m)}, t_z^{(m)}, \\ &X_1, Y_1, Z_1, \ldots, X_m, Y_m, Z_m\big)^{\mathrm{T}}. \end{aligned} \tag{7}$$

Expressions (1) of the residual errors in the image plane provide $2mn$ equations for solving vector $\mathbf{\Phi}$ with a redundancy equal to

$$r = 2mn - (8 + 6m + 3n). \tag{8}$$

Thus, even if the calibration point coordinates are included in the vector $\mathbf{\Phi}$ of the parameters, recording between three and ten views (depending on the number n of the calibration points) guarantees a redundancy high enough to be relevant for a least mean square procedure.

2.3. Solving the problem

The problem is to estimate vector $\mathbf{\Phi}$ by minimizing the sum of the square residual errors:

$$S = \sum_{i=1}^{n} \sum_{j=1}^{m} \left(\varepsilon \mathrm{u}_{i,j}^2 + \varepsilon \mathrm{v}_{i,j}^2\right). \tag{9}$$

This optimization is done from image coordinates $(\mathrm{u}_{i,j}, \mathrm{v}_{i,j})$ of n calibration points $(X_i, Y_i, Z_i)_{i=1,\ldots,n}$, measured in m views ($j = 1, \ldots, m$). As residual errors are nonlinear functions of $\mathbf{\Phi}$, the minimization is a nonlinear optimization problem. One way of solving the problem is to linearize (1) with some initial vector $\mathbf{\Phi}^{(0)}$, to solve for $\Delta\mathbf{\Phi}$ then to add $\Delta\mathbf{\Phi}$ to $\mathbf{\Phi}^{(0)}$ as the new initial vector and repeat the process until a certain convergence is satisfied.

The $2mn$ linearized residual error equations (1) can be written in the matrix form

$$\mathbf{E} = \mathbf{L} + \mathbf{J}\,\Delta\mathbf{\Phi}, \tag{10}$$

where $\mathbf{L}$ is the residual error matrix at $\mathbf{\Phi} = \mathbf{\Phi}^{(0)}$ and $\mathbf{J}$ is its Jacobian matrix at this point. The least-squares solution to (10) is given by

$$\widehat{\Delta\mathbf{\Phi}} = (\mathbf{J}^{\mathrm{T}}\mathbf{W}\mathbf{J})^{-1}\mathbf{J}^{\mathrm{T}}\mathbf{W}\mathbf{L}, \tag{11}$$

where $\mathbf{W}$ is the weight matrix of the measurements. The estimate of residual vector $\mathbf{E}$ can be computed as

$$\hat{\mathbf{E}} = [\mathbf{I} + \mathbf{J}(\mathbf{J}^{\mathrm{T}}\mathbf{W}\mathbf{J})^{-1}\mathbf{J}^{\mathrm{T}}\mathbf{W}]\mathbf{L} \tag{12}$$

and the estimate of the so-called *standard error of unit weight* as

$$\hat{\sigma}_0^2 = \frac{\hat{\mathbf{E}}^{\mathrm{T}}\mathbf{W}\hat{\mathbf{E}}}{r}, \tag{13}$$

where $\hat{\sigma}_0$ is the *a posteriori* estimate of the standard deviation σ_0 of the image coordinates by assuming that the model is correct and there are no systematic errors.

For each individual parameter Φ_k, the estimate of its precision is given by

$$\hat{\sigma}_{\Phi_k}^2 = \hat{\sigma}_0^2 \hat{c}_{kk}, \tag{14}$$

where $\hat{c}_{kk}$ is the estimate of the kth diagonal element of the *covariance* matrix $\mathbf{C}_\Phi$ of the parameters, estimated as

$$\hat{\mathbf{C}}_\Phi = (\mathbf{J}^{\mathrm{T}}\mathbf{W}\mathbf{J})^{-1}. \tag{15}$$

3. An easy protocol for Scheimpflug self-calibration

In the Scheimpflug condition, the planes of the near and far limits of the depth of field are no longer parallel to the plane of sharp focus. The region of acceptable definition is in fact wedge-shaped [18]. The sharp edge of the wedge (Hinge line) is a line in the object plane in the object space, parallel to the lens plane at a distance equal to the image distance p_i (figure 1). In standard PIV conditions, images remain focused provided that the calibration target located at the centre of the field of view is not rotated more than about 10°. This limit

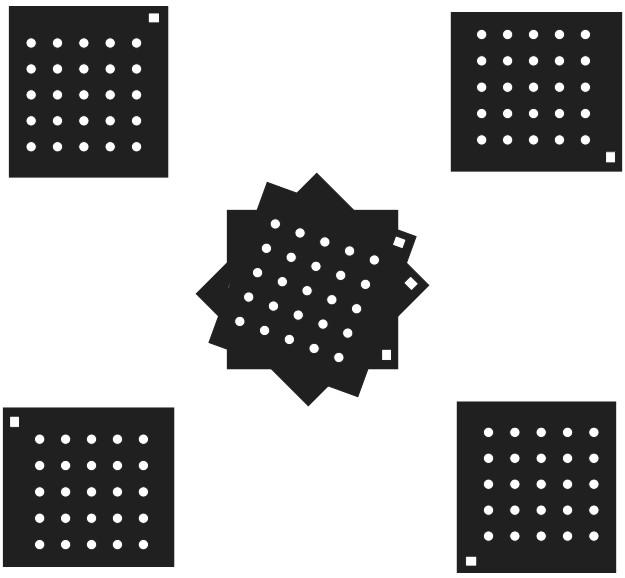

Figure 3. Superimposition of the side views and central views of the calibration target in the field.

decreases when the target is moved towards the Hinge line side.

The target can be hand-positioned on this side in the depth of field and in a corner of the field of view. Then, in-plane translations can be roughly applied on the target in order to cover the other corners and the centre of the field of view. m_2 views recorded at the corners in order to get a good estimate of the distortion coefficients a_1, a_2, a_3 complete m_1 views recorded at the centre (figure 3). After recording the first view at the centre, the $(m_1 - 1)$ other central views can be obtained by in-plane rotations. A printed flat target of n dots can serve as the calibration object for the bundle adjustment. The coordinates of the calibration points are optimized together with the camera parameters from the $m = m_1 + m_2$ views of the target. A Levenberg–Marquardt procedure can be applied to an initial vector $\mathbf{\Phi}^{(0)}$ after the detection of coordinates $(\mathrm{u}_{i,j}, \mathrm{v}_{i,j})$ of the n calibration points in the m views.

For initialization of vector $\mathbf{\Phi}$, the coordinates X_i, Y_i, Z_i of the calibration points can be read directly from the print file of the target. For the parameters of the camera model (see section 2.1) one can proceed as follows. Image distances $p_{i\,x}$ and $p_{i\,y}$ are obtained by dividing the specified focal length f by the pixel sizes $\mathrm{d}x$ and $\mathrm{d}y$, respectively. Coordinates (u_0, v_0) of the image centre are initialized with the pixel coordinates of the middle of the matrix sensor. Distortion coefficients a_1, a_2, a_3 are set to zero. The Scheimpflug tilt θ is computed from (4) with approximate values for M and β. Extrinsic parameters $\alpha^{(j)}$, $\beta^{(j)}$, $\gamma^{(j)}$, $t_x^{(j)}$, $t_y^{(j)}$, $t_z^{(j)}$ are obtained with DeMenthon and Davis' algorithm [19].

4. Experimental results

The bundle adjustment technique has been claimed to simplify the calibration of Scheimpflug cameras by handpositioning a printed flat target in a sheet of the depth of field. However, two critical points have to be studied for this purpose: what is the precision required for the calibration target and how many views are really useful. The suggested protocol was tested with two $1/2''$ CCD cameras having 1024×768 square pixels of size $\mathrm{d}x = \mathrm{d}y = 6.25\ \mu$m. The CCD cameras equipped with $f = 50$ mm lenses ($f/\mathrm{d}x = 8000$ pixels) were located at a working distance $p_0 = 1$ m, respectively, viewing under $\beta = \pm 45°$. It corresponds to a nominal magnification $M = 0.05$ and a Scheimpflug tilt $\theta = 2.86°$. A flat grid of 5×5 dots provided $n = 25$ calibration points and redundancy $r = 44m - 83$. Two views ($m = 2$) are then required at a minimum. Simulated data were used to assess the sensitivity of both the location error on the calibration point coordinates and the number of views. Afterwards, the reliability of the calibration protocol was tested in real conditions. The reconstruction of a metrological target is first considered to test the target handpositioning in Scheimpflug camera self-calibration. Image rectification is then considered to test the ability to correct the misalignment between the reference plane and a light sheet with roughly-known features.

4.1. Simulated data

Handpositioning was simulated by randomly selecting (according to Gaussian distributions) the pose of the calibration target within 5° in rotation and 10 mm in translation with respect to the focal plane. The distortion rate was fixed such that it represents an amount of 6.5 pixels at the edges of images ($a_1 = 3$). For each test, 100 trials were done: initial values were randomly choosen according to a uniform distribution in the range of $[40°,\ 50°]$ for β, [45 mm, 55 mm] for f and in a circle of radius 30 pixels around the matrix centre for $(u_0,\ v_0)$.

4.1.1. Sensitivity to errors on the calibration points. The coordinates of the calibration points $\mathbf{X}_i$ and their images were contaminated by Gaussian white noise, with an increasing standard deviation σ_{XYZ} at given σ_{uv}. Five views were used for the calibration: one view at the centre ($m_1 = 1$) and one view at each corner ($m_2 = 4$). The estimates of the image distance $p_{i\,x}$ and the Scheimpflug tilt θ are reported with their standard deviations in table 1. The unitary scale factor k on the target geometry defined as the ratio between the mean spacing distance measured after reconstruction and the spacing distance is also reported in table 1.

One can note that an error of 10 mm on the calibration points has no influence. On the contrary, accurate image detection is required to get good estimates of the parameters: the detection error has to be less than 0.05 pixel. This result agrees with the result obtained for the bundle adjustment of standard cameras in computer vision [20]. With a detection precision greater than or equal to 0.05 pixel, the unitary scale factor becomes distant from 1 and the estimation of the parameters is no longer precise.

4.1.2. Sensitivity to the number of views. According to the previous section, the image detection error was here assumed to be $\sigma_{uv} = 0.02$ pixel. The error on calibration points was set to $\sigma_{XYZ} = 1$ mm, this value being easy to reach in practice. $m = m_1 + m_2$ views were computed, with a single view at the centre until $m = 5$ views and with a single view per corner and several rotations at the centre for

Table 1. Sensitivity to errors on the coordinates of the calibration points for different levels of image detection errors ($m = 5$).

		$\sigma_{uv} = 0.01$ pixel		
σ_{XYZ} (mm)	0.01	0.1	1	10
p_{i_x} (pixel)	8001.22 ± 3.58	7999.08 ± 5.79	7998.67 ± 6.38	8002.11 ± 6.69
θ (degree)	2.86 ± 0.00	2.86 ± 0.01	2.86 ± 0.01	2.86 ± 0.01
k	1.00 ± 0.00	1.00 ± 0.00	1.01 ± 0.00	0.99 ± 0.00
		$\sigma_{uv} = 0.02$ pixel		
σ_{XYZ} (mm)	0.01	0.1	1	10
p_{i_x} (pixel)	8001.35 ± 4.28	7999.45 ± 6.32	8002.29 ± 6.36	7998.01 ± 7.54
θ (degree)	2.86 ± 0.01	2.86 ± 0.01	2.86 ± 0.01	2.86 ± 0.01
k	1.00 ± 0.00	1.00 ± 0.00	1.01 ± 0.00	0.99 ± 0.00
		$\sigma_{uv} = 0.05$ pixel		
σ_{XYZ} (mm)	0.01	0.1	1	10
p_{i_x} (pixel)	7486.09 ± 179.00	8633.64 ± 186.60	7293.79 ± 238.40	8757.32 ± 244.70
θ (degree)	3.59 ± 000.34	3.71 ± 000.56	3.69 ± 000.54	3.78 ± 000.77
k	1.04 ± 000.02	1.05 ± 000.02	0.93 ± 000.03	0.91 ± 000.03
		$\sigma_{uv} = 0.1$ pixel		
σ_{XYZ} (mm)	0.01	0.1	1	10
p_{i_x} (pixel)	8613.42 ± 218.00	8615.79 ± 394.40	8918.13 ± 454.80	9185.62 ± 649.20
θ (degree)	3.61 ± 000.25	3.61 ± 000.26	3.85 ± 000.34	3.91 ± 000.57
k	1.03 ± 000.01	0.95 ± 000.03	0.93 ± 000.03	0.90 ± 000.04

Table 2. Sensitivity to the number of views for $\sigma_{XYZ} = 1$ mm and $\sigma_{uv} = 0.02$ pixel.

m	p_{i_x} (pixel)	θ (degree)	k
2	364.92 ± 128.34	3.74 ± 0.24	0.91 ± 0.04
3	8269.85 ± 112.42	2.93 ± 0.38	0.97 ± 0.04
4	7987.02 ± 103.42	2.81 ± 0.08	0.98 ± 0.00
5	8002.29 ± 006.36	2.86 ± 0.01	1.01 ± 0.00
8	8002.16 ± 007.62	2.86 ± 0.02	1.01 ± 0.00
10	8001.92 ± 011.13	2.86 ± 0.02	1.01 ± 0.00

$m > 5$ views. As before, the estimates of both the image distance p_{i_x} and the Scheimpflug tilt θ are reported with their standard deviations in table 2 together with the scale factor k. Accurate results are obtained from $m = 5$ views and also for the other intrinsic parameters. The distortion coefficients and the image centre are retrieved concentrated on coefficient a_1 and close to the matrix centre, respectively. For example, the following values were measured for $m = 5$: $a_1 = 2.71 \pm 0.30$, $a_2 = 0.03 \pm 0.01$, $a_3 = 0.05 \pm 0.02$ and $u_0 = 511.81 \pm 2.13$ pixels, $v_0 = 384.68 \pm 1.06$ pixels. Similar results are obtained for $m = 8$ and $m = 10$ views.

4.2. Real data

A pair of CCD cameras (Sony XC 700) separately mounted on a Scheimpflug support device were self-calibrated. Each camera was equipped with a standard $f = 50$ mm lens (Canon Series E). The aperture number was $f^{\#} = 1.8$.

4.2.1. Test of target handpositioning A precision dot grid target (Melles Griot 59 TDT 115) was hand-positioned at different locations in the field and self-calibration was carried out as mentioned in section 3. This target was also used as a test object to reconstruct. Only 25 dots were selected from the 1089 chrome-on-glass reticles (dot diameter 1500 ± 15 μm). At each position of the target, one view was recorded: one view per corner ($m_2 = 4$) and six views at the centre after rotations in steps of 60°. Self-calibration was performed using all the views ($m = 10$). A second self-calibration was carried out using a subset reduced to the four side views and only one central view ($m = 5$). Image detection was performed according to the algorithm of dot-centre detection given in [15].

Table 3. Intrinsic parameters of the right camera after self-calibration.

$m = 10$	
p_{i_x}, p_{i_y} (pixel)	7918.72 ± 0.48
u_0 (pixel)	491.91 ± 0.26
v_0 (pixel)	382.53 ± 0.36
a_1	2.92 ± 0.12
a_2	-0.11 ± 0.06
a_3	-0.13 ± 0.11
θ (degree)	3.06 ± 0.21
Residual = 0.03 pixel	
$m = 5$	
p_{i_x}, p_{i_y} (pixel)	7924.70 ± 0.53
u_0 (pixel)	495.41 ± 0.25
v_0 (pixel)	380.62 ± 0.47
a_1	2.95 ± 0.14
a_2	-0.09 ± 0.09
a_3	0.1 ± 0.17
θ (degree)	3.07 ± 0.23
Residual = 0.03 pixel	

For each camera, reliable results are obtained for ten and five views (tables 3 and 4). The confidence intervals intersect well for u_0, v_0, a_1, a_2, a_3, θ. Concerning image distances p_{i_x}, p_{i_y}, their estimates from $m = 5$ views differ from those obtained from $m = 10$ views with a deviation inferior to 0.1% of the focal length. 0.1% is also the low deviation we obtained for image distances when self-calibration was compared with calibration (coordinates X_i, Y_i, Z_i being fixed to the coordinates of the nodes of the subjacent regular grid). In all the cases, the ratio p_{i_x}/p_{i_y} is equal to unity which agrees with the fact that the pixels of the sensor are square. Furthermore, the residual error given by the optimization procedure is about 0.03 pixel. It agrees with the precision

Table 4. Intrinsic parameters of the left camera after self-calibration.

$m = 10$	
p_{ix}, p_{iy} (pixel)	7938.94 ± 0.62
u_0 (pixel)	501.12 ± 0.29
v_0 (pixel)	387.49 ± 0.34
a_1	2.76 ± 0.18
a_2	-0.09 ± 0.15
a_3	0.12 ± 0.12
θ (degree)	2.93 ± 0.24
Residual = 0.03 pixel	
$m = 5$	
p_{ix}, p_{iy} (pixel)	7941.05 ± 0.68
u_0 (pixel)	499.76 ± 0.28
v_0 (pixel)	383.97 ± 0.34
a_1	2.79 ± 0.22
a_2	-0.16 ± 0.17
a_3	0.08 ± 0.11
θ (degree)	2.97 ± 0.21
Residual = 0.04 pixel	

required for image detection and corresponds to a precision of the order of 1 μm in the object space at this magnitude.

The target should be accurately reconstructible from a stereo pair of views not used in the self-calibration procedure. The values of the intrinsic parameters optimized from $m = 5$ views were used for this reconstruction (tables 3 and 4). The spacing in the reconstructed grid is 3018 ± 11 μm according to the X-axis and 3027 ± 17 μm according to the Y-axis. These measurements agree with the specification of the spacing distance: 3000 ± 10 μm. In addition, the Z-coordinates are close to zero within ± 1 μm which is consistent with the manufacturing process of the target (deposition of a thin layer of metal).

4.2.2. Test of misalignment correction with roughly-known features To check for misalignment between the PIV laser sheet and the reference plane used for self-calibration, in addition to the technique commented in the introduction, let us introduce a different approach which is being tested here: the rectification of images of circular shapes after the Scheimpflug camera's self-calibration.

The self-calibration of the Scheimpflug cameras was performed as previously but with five views of a 2D roughly-known plate. The calibration pattern is here a 5×5 dot grid which was laser-printed on a piece of paper stuck to the plate. The *a priori* parameters of the grid are 2 mm for the dot diameter and 5 mm for the spacing between the dots. The residual errors after self-calibration are in the same order as in the previous test carried out in real conditions.

An argon laser sheet was located in the depth of field of the cameras. The laser plane equation can be obtained by recovering inter-image homography H_{21} from homologous image pairs of some feature points after the correction of the image distortions [13]. Cross-sections of two 20–25 mm spherical soap bubbles filled with smoke were illuminated by the laser sheet (of about 1 mm thick). These cross-sections marked the laser plane as two circular dots which can be imaged into large ellipses in image planes. Points associated with the bitangents of the two dots (i.e. the tangents common to the pair of dots) were considered as feature points [21].

Images corresponding to a new location of the bubbles should now be rectifiable. Indeed the inter-image homography can be expressed with the scene–image homographies: $H_{21} = H_2 H_1^{-1}$ and each scene–image homography ($j = 1, 2$) can be reduced to the product of image rectification Q_j with similarity S_j in the planar scene: $H_j = Q_j^{-1} S_j$ [22]. Thus, the inter-image homography can be expressed as $H_{21} = Q_2^{-1} S_{21} Q_1$ where $S_{21} = S_2 S_1$ is a similarity, and the ellipses in images 1 and 2 can be rectified into circles (within a similarity) if the laser plane has been correctly determined. Images corresponding to a new location of the bubbles were successfully rectified. The eccentricity measurements give 1.12 and 1.11 in images 1 and 2, respectively, then 1.00 after rectification.

5. Conclusion

This paper presents a protocol which allows the self-calibration of Scheimpflug cameras with only five views of a roughly-known planar target hand-positioned in the depth of field. The five views cover the field of view. The calibration pattern can be known within 1–10 mm provided that the precision of the detection of the feature points in images is better than 0.05 pixel. This requirement is in agreement with the classical requirement of bundle adjustment techniques in computer vision. Specific algorithms exist for appropriate image detection, depending on the geometry of the calibration pattern and the feature points to be detected. Therefore, the calibration patterns can be generated by the end user with standard means such as a laser printer or a generator of spherical bubbles. This last possibility could lead to a special calibration.

Acknowledgments

The authors wish to thank J F Menudet from the University of Saint-Etienne and T Filali from the University of Monastir for their help in the real experiments.

References

[1] Hinsch K D, Hinrichs H, Roshop A and Dreesen F 1993 Holograpic and stereoscopic advance in 3D PIV *Holographic Particle Image Velocimetry, Proc. Fluids Engineering Division* vol 148, ed E P Rood (Washington, DC: American Society of Mechnical Engineers) pp 33–6

[2] Prasad A K and Jens K 1995 Scheimpflug stereocamera for particle image velocimetry in liquid flow *Appl. Opt.* **34** 7092–9

[3] Westerweel J and Van Oord J 1999 Stereoscopic PIV measurements in a turbulent boundary layer *Particle Image Velocimetry: Progress Towards Industrial Application* ed M Stanislas, J Kompenhans and J Westerweel (Dordrecht: Kluwer) pp 459–78

[4] Van Oord J 1997 The design of a stereoscopic DPIV system *Delft University of Technology Report* MEAH-161

[5] Willert C 1997 Stereoscopic digital particle image velocimetry for application in wind tunnel flows *Meas. Sci. Technol.* **8** 1465–79

[6] Lawson N and Wu J 1997 Three-dimensional particle image velocimetry: experimental error analysis of digital angular stereoscopic system *Meas. Sci. Technol.* **8** 1455–64

[7] Naqwi A 2000 Distortion compensation for PIV systems *10th Int. Symp. Application of Laser Technique to Fluid Mechanics (Lisbon, Portugal)* paper 6.2

[8] Soloff S, Adrian R and Liu Z C 1997 Distortion compensation for generalized stereoscopic particle image velocimetry *Meas. Sci. Technol.* **8** 1441–54
[9] Quénot G, Rambert A, Lusseyran F and Gougat P 2001 Simple and accurate PIV camera calibration using a single target image and camera focal length *4th Int. Symp. Particle Image Velocimetry (Gottingen, Germany)* paper 1040
[10] Raffel M, Willert C and Kompenhans J 1998 *Particle Image Velocimetry: A Practical Guide* (Berlin: Springer)
[11] Coudert S and Schon J P 2001 Back-projection algorithm with misalignment correction for 2D3C stereoscopic PIV *Meas. Sci. Technol.* **12** 1371–81
[12] Scarano F, David L, Bsibsi M, Calluaud D and Akkermans R A D 2005 Comparison of two S-PIV techniques: pinhole versus image dewarping and misaligment correction *Exp. Fluids* **39** 257–66
[13] Fournel T, Lavest J M, Coudert S and Collange F 2003 Self-calibration of PIV video-cameras in Scheimpflug condition *Proc. EuroPIV 2 Workshop. Particle Image Velocimetry: Recent Improvements (Zaragoza, Spain)* ed M Stanislas, J Westerweel and J Kompenhans (Berlin: Springer) pp 391–405
[14] Wieneke B 2005 Stereo-PIV using self-calibration on particle images *Exp. Fluids* **39** 267–80
[15] Lavest J M, Viala M and Dhome M 1998 Do we really need an accurate calibration pattern to achieve a reliable camera calibration *Proc. ECCV98 (Freiburg, Germany)* pp 158–74
[16] Triggs W, McLauchlan P, Hartly R and Fitzgibbon 2000 *Vision Algorithms: Theory and Practice* (Berlin: Springer) pp 298–375
[17] American Society for Photogrammetry 1984 *Manual of Photogrammetry* 4th edn
[18] Merklinger H M 1996 View camera focus and depth of field *View Camera Mag.* 56–8
[19] Davis L S and DeMenthon D F 1995 Model based object pose in 25 lines of code *Int. J. Comput. Vis.* **15** 123–41
[20] Plancke P 1977 Calibration of vision systems *European Space Agency Report* WPB5-T1
[21] Fournel T, Louhichi H, Barat C and Menudet J F 2006 Scheimpflug self-calibration based on tangency points *Int. Symp. Flow Visualization (Gottingen, Germany)* paper
[22] Liebowitz D 2001 Camera calibration and reconstruction of geometry from images *PhD Thesis* University of Oxford